ELECTRONIC SUPPLEMENTARY INFORMATION

Investigation of the inherent characteristics of copper(II) Schiff base complexes as antimicrobial agents

Thasnim P Mohammed,[a] Abinaya Sushana Thennarasu,[a] Ravi Jothi,[b] Shanmugaraj Gowrishankar,[b] Marappan Velusamy,[c] Suman Patra[d] and Muniyandi Sankaralingam*[a]

[a]*Bioinspired & Biomimetic Inorganic Chemistry Laboratory, Department of Chemistry, National Institute of Technology Calicut, Kozhikode, Kerala 673601 India.*

[b]*Department of Biotechnology, Science Campus, Alagappa University, Karaikudi – 630 003, Tamil Nadu, India.*

[c]*Department of Chemistry, North Eastern Hill University, Shillong-793022, India.*

[d]*School of Chemical Sciences, Indian Association for the Cultivation of Science, Kolkata 700032, India*

*Corresponding author e-mail: msankaralingam@nitc.ac.in; sankarjan06@gmail.com

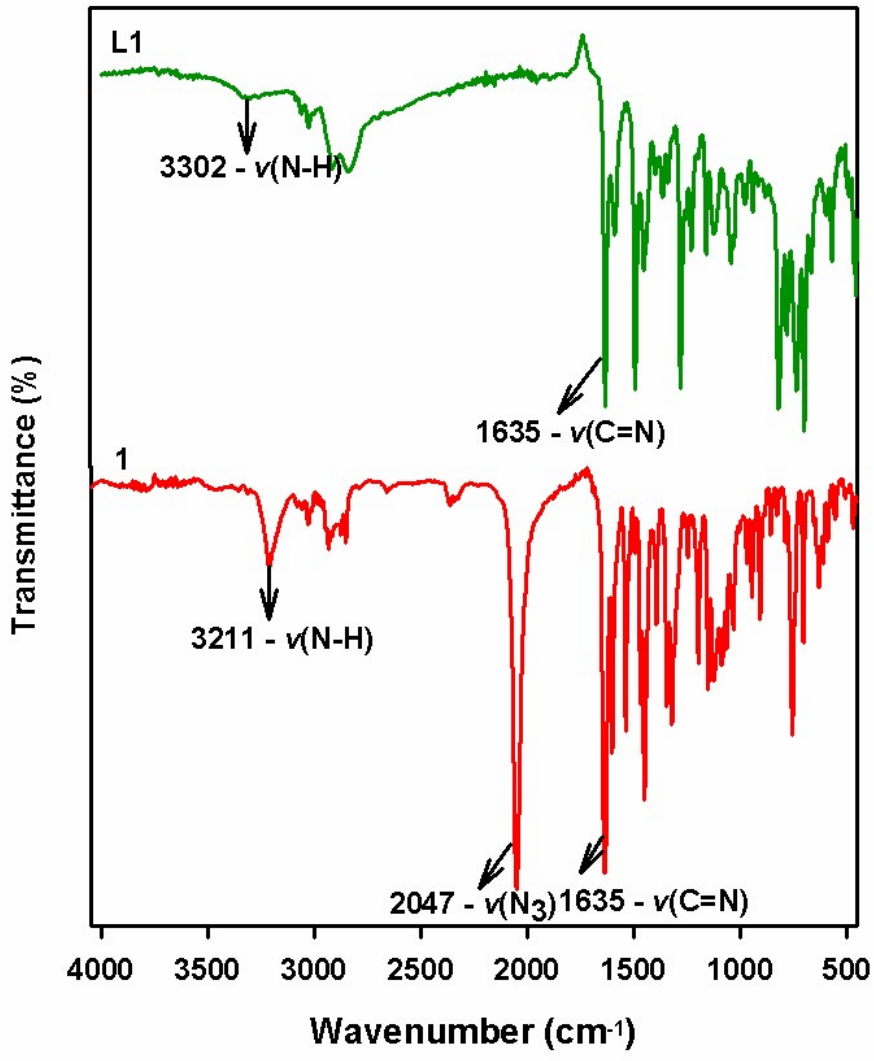

Fig. S1. ATR spectra of ligand **L1**(H) and IR spectra of complex **1.**

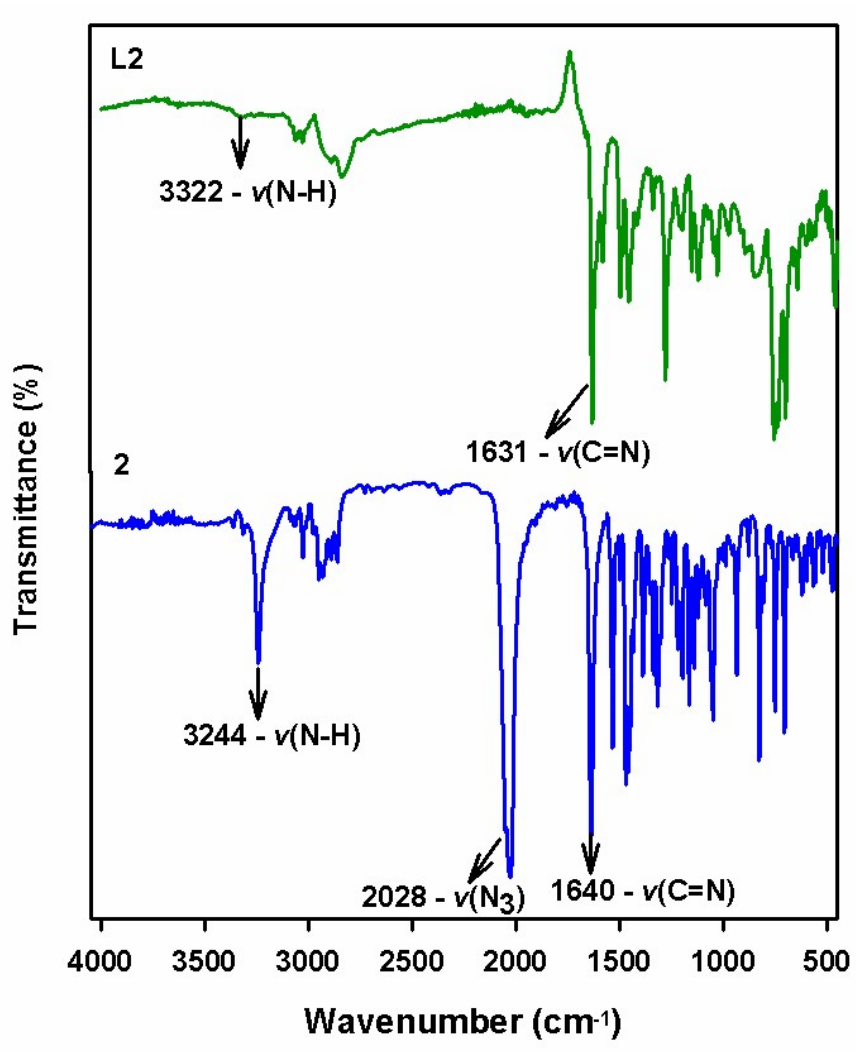

Fig. S2. ATR spectra of ligand **L2**(H) and IR spectra of complex **2.**

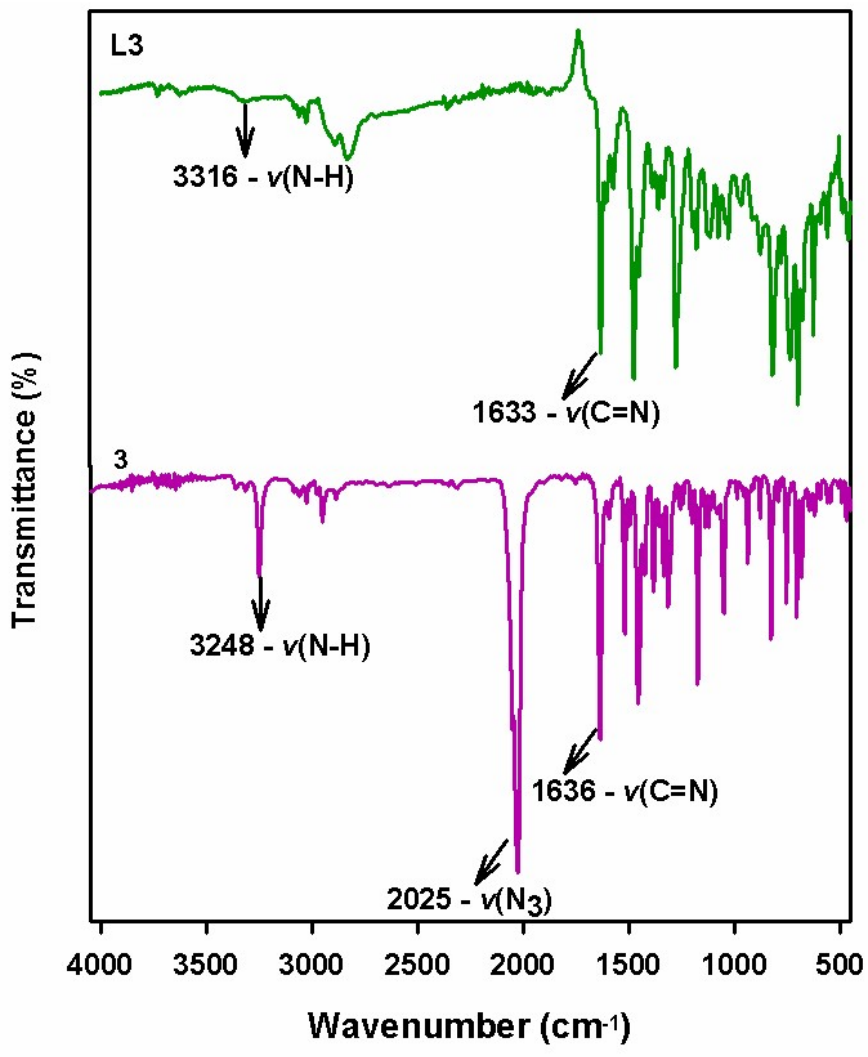

Fig. S3. ATR spectra of ligand **L3**(H) and IR spectra of complex **3.**

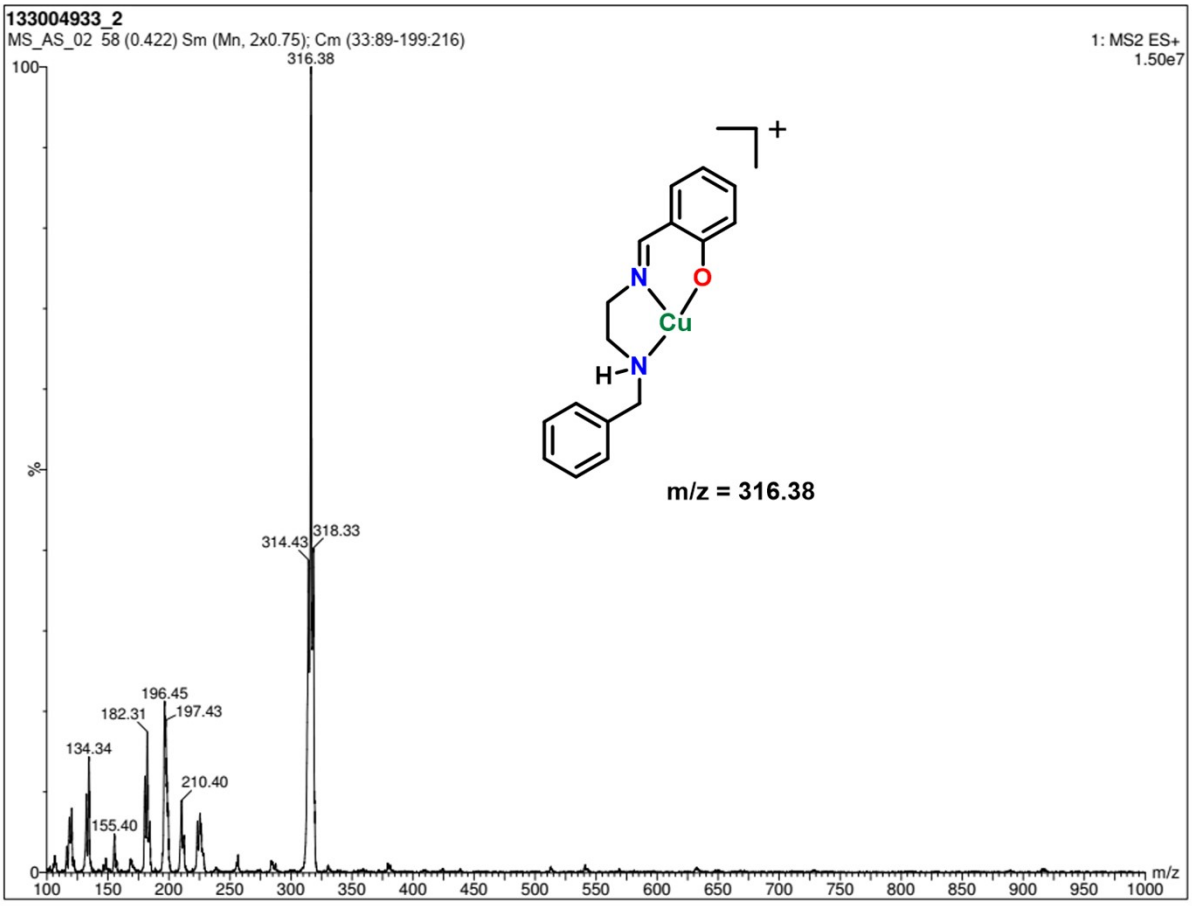

Fig. S4. Mass spectral data of complex **1.**

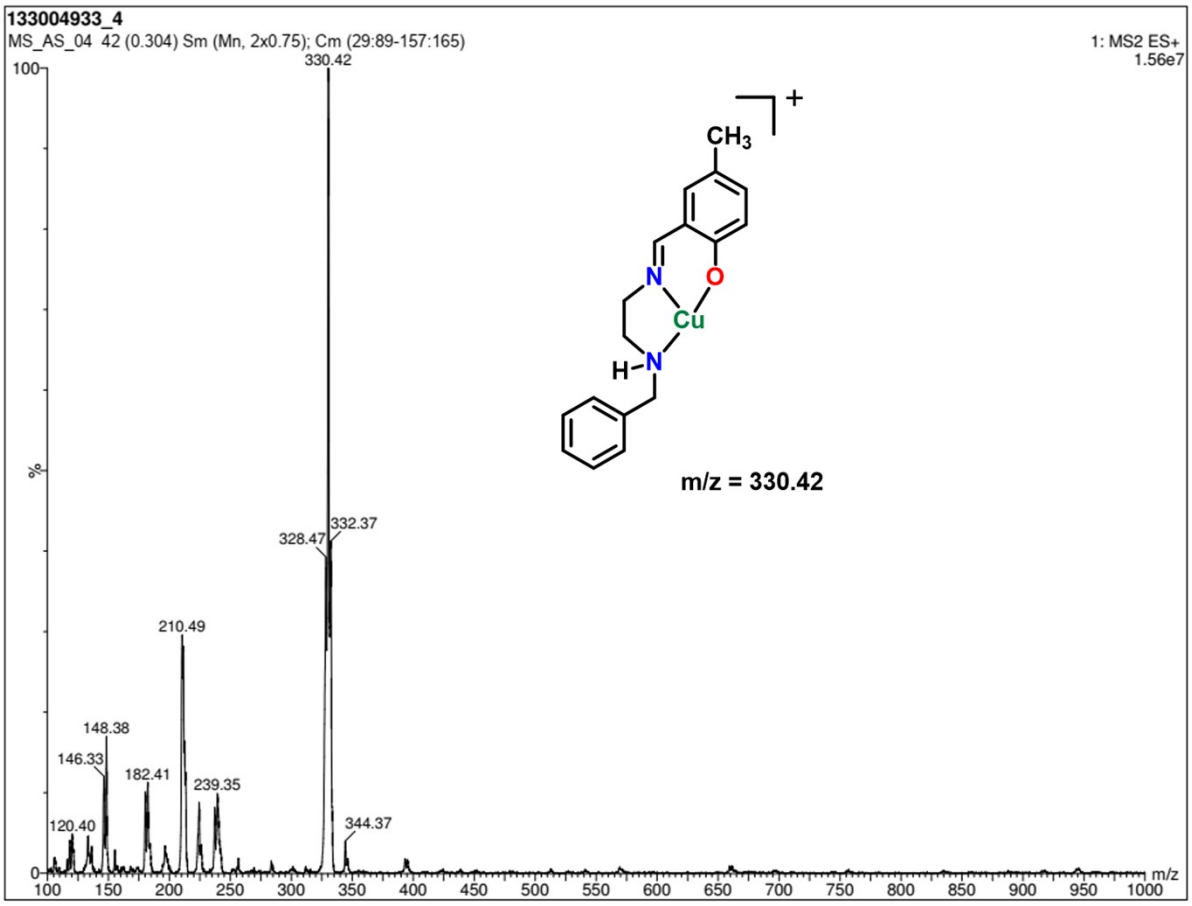

Fig. S5. Mass spectral data of complex **2.**

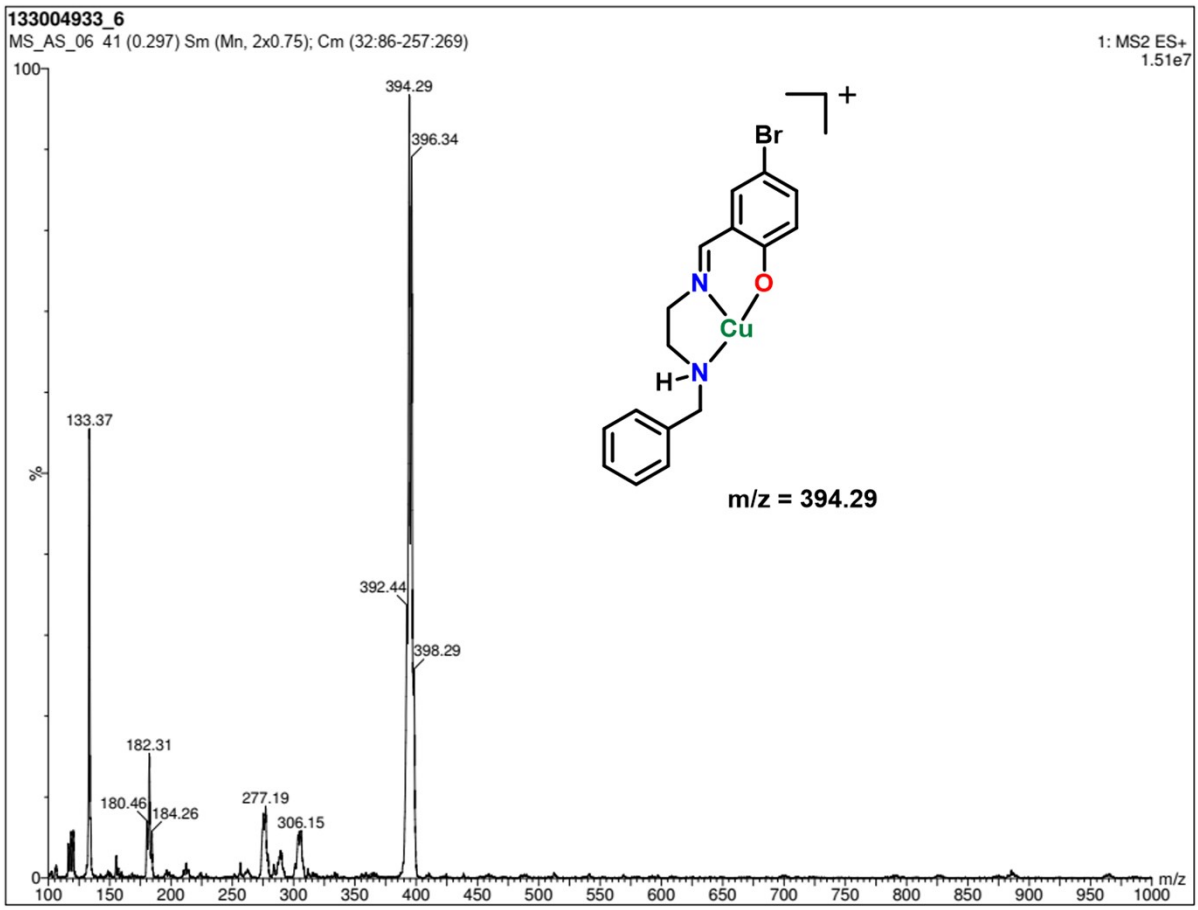

Fig. S6. Mass spectral data of complex **3.**

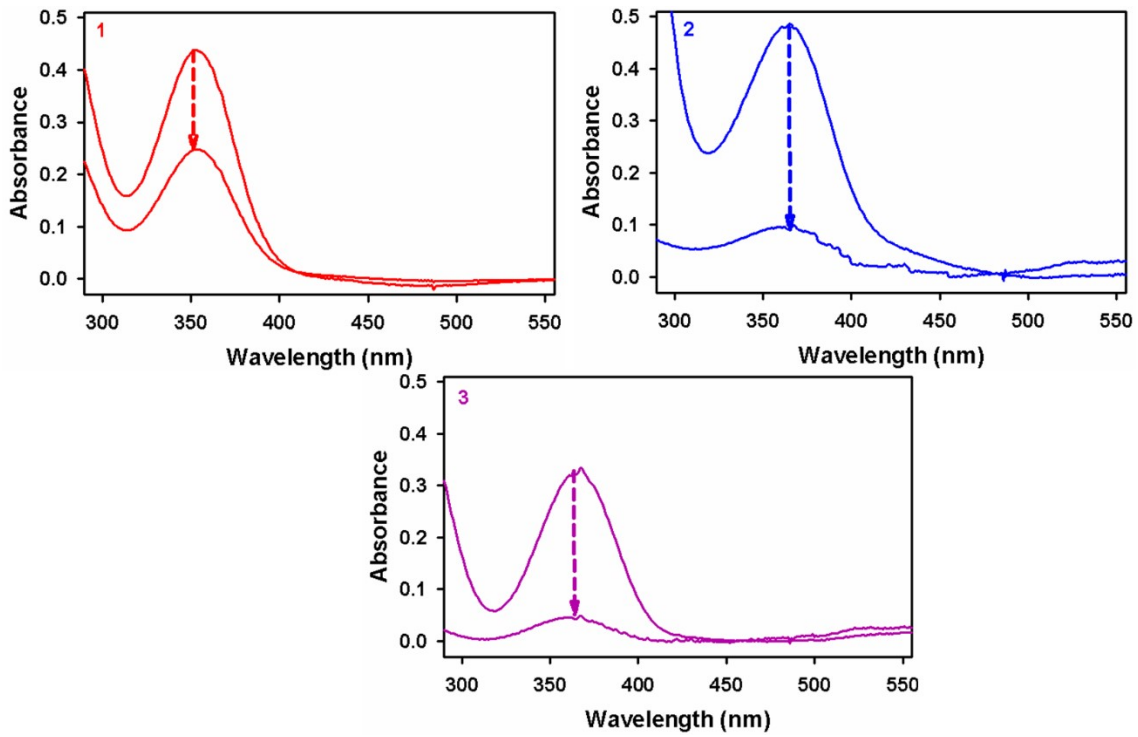

Fig. S7. UV-visible spectra of complexes **1-3** in aqueous phase before (upper spectra) and after (lower spectra) extraction with the water-saturated 1-octanol.

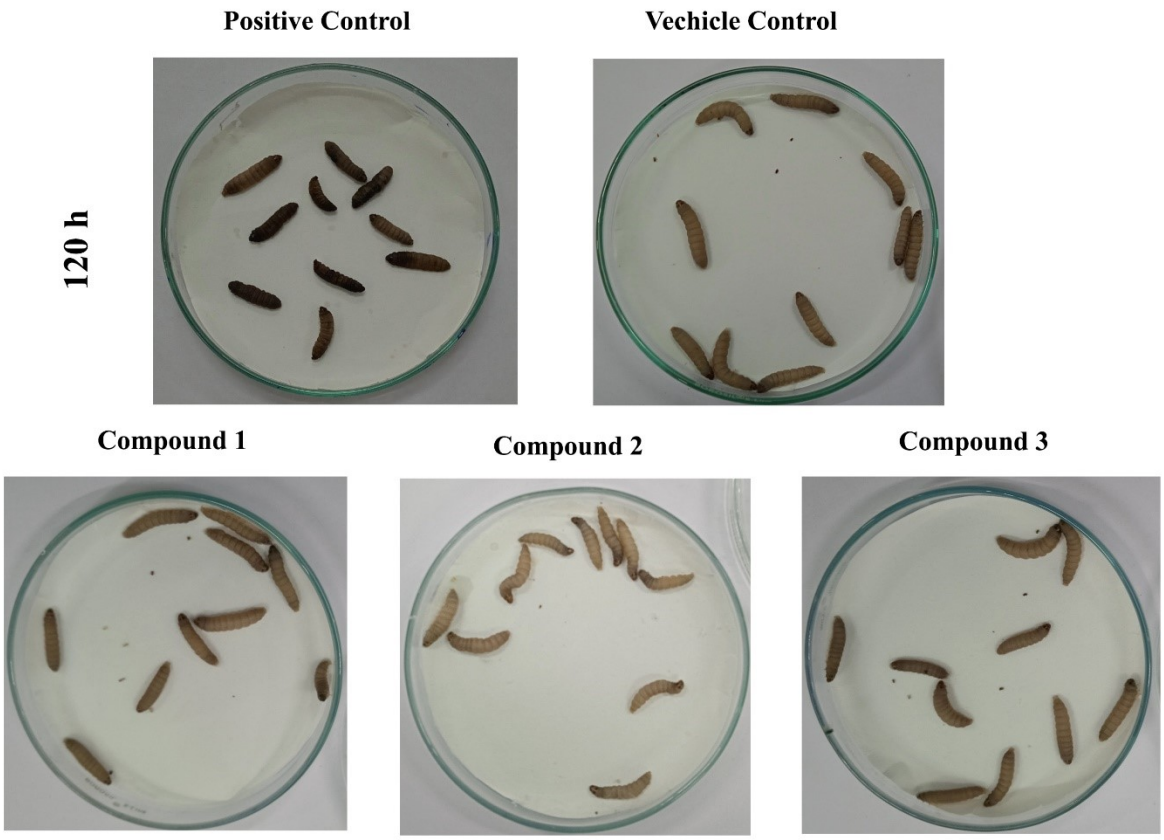

Fig. S8. The toxicity study using the larvae, *Galleria mellonella* reveals the positive control injected larvae with methanol are died after 120 h, whereas the larvae in DMSO-injected vehicle group and those injected with complexes (**1-3**) are alive.

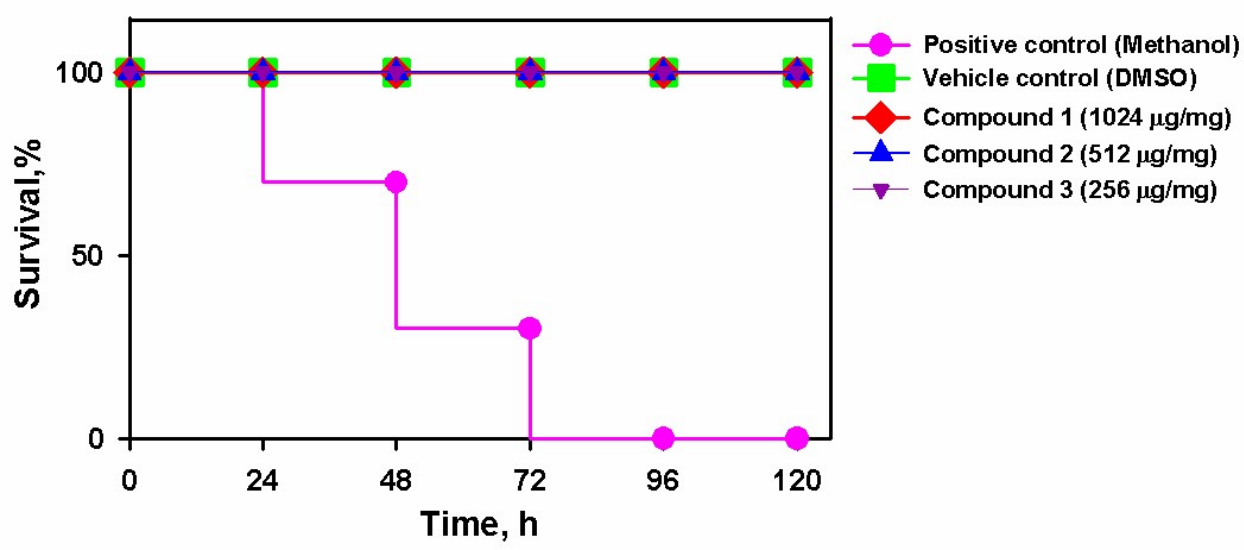

Fig. S9. The survival percent of complexes at different intervals of time indicating the complexes (**1**-**3**) are 100% non-toxic.

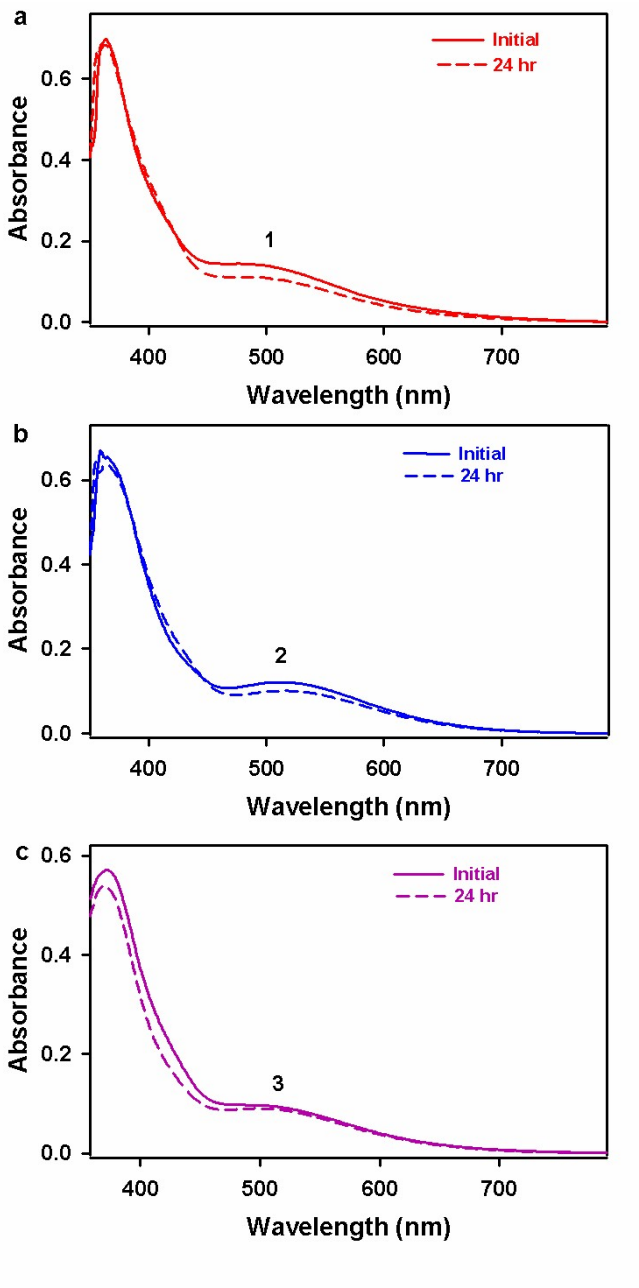

Fig. S10. UV-vis spectra of complexes (**a-c**) recorded in YEPD at different time intervals under identical conditions followed for microbial studies. Difference spectra of complexes were plotted from the spectra of broth.

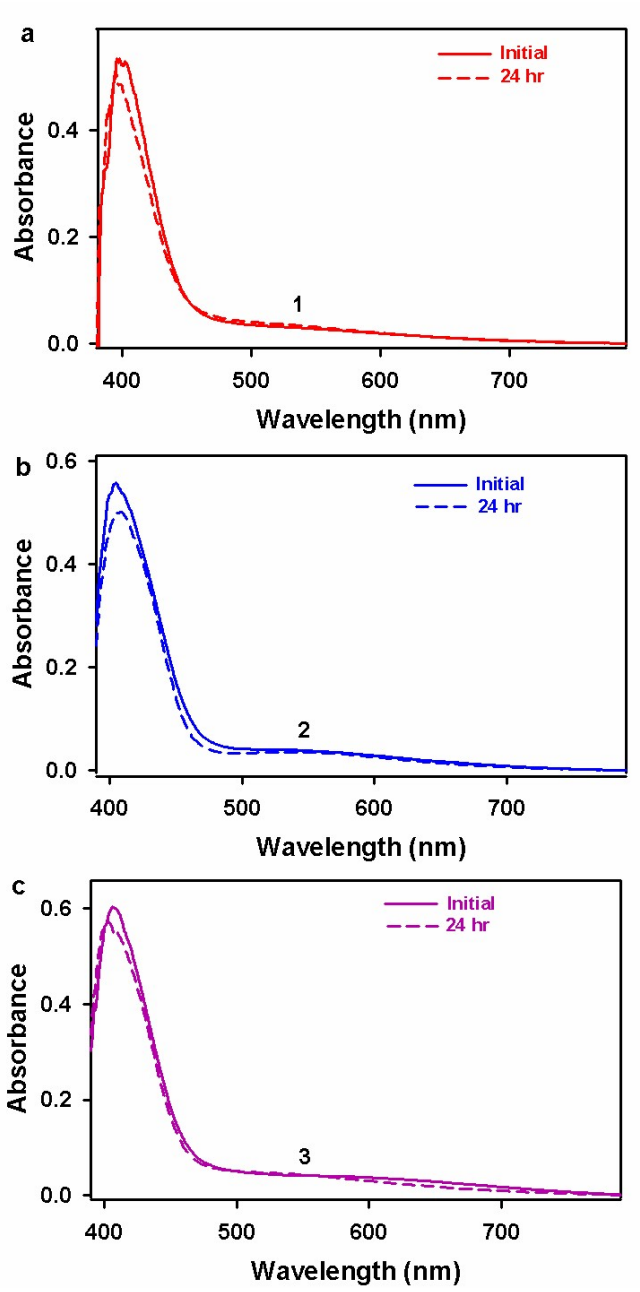

Fig. S11. UV-vis spectra of complexes (**a-c**) recorded in BHI at different time intervals under identical conditions followed for microbial studies. Difference spectra of complexes were plotted from the spectra of broth.

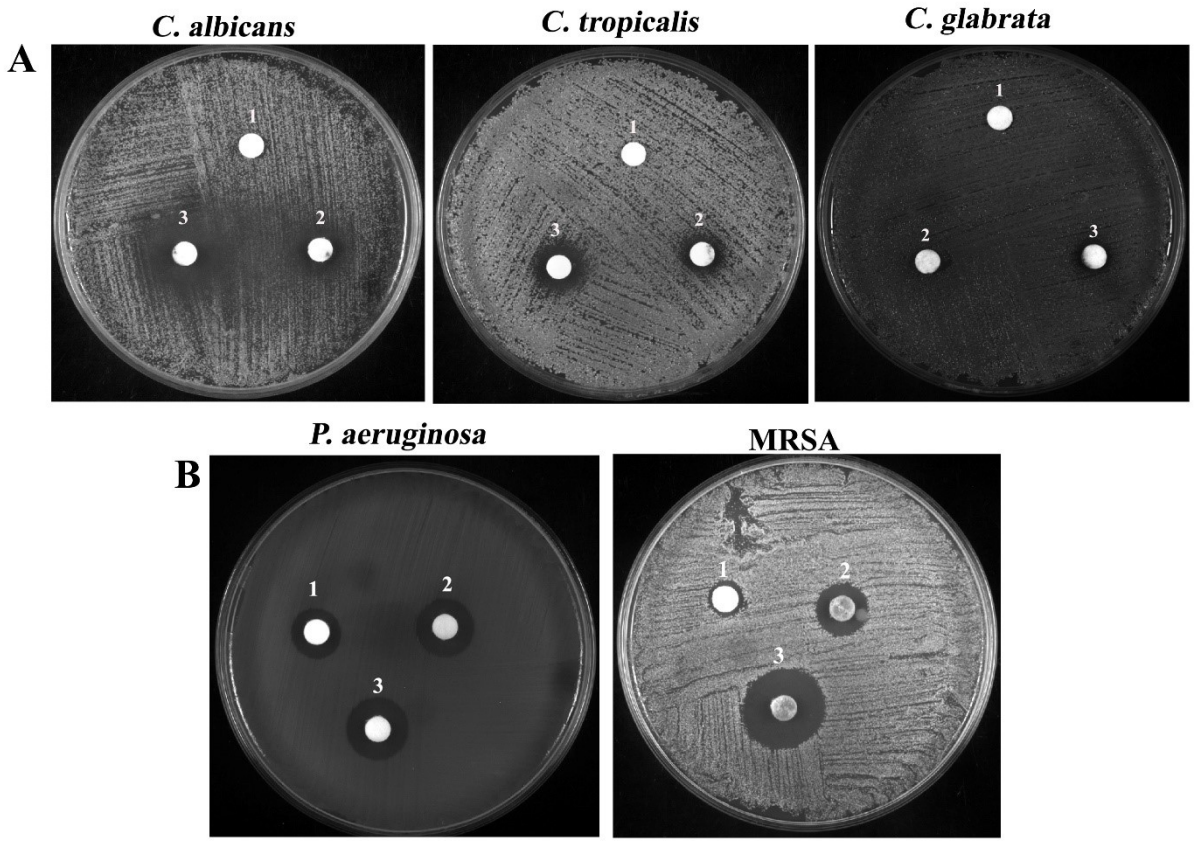

Fig. S12. The representative plate image showcases the effect of test complexes against used **(A)** fungal and **(B)** bacterial strains as determined through disk diffusion technique. The complexes are marked with **1**, **2**, and **3** in the wells.

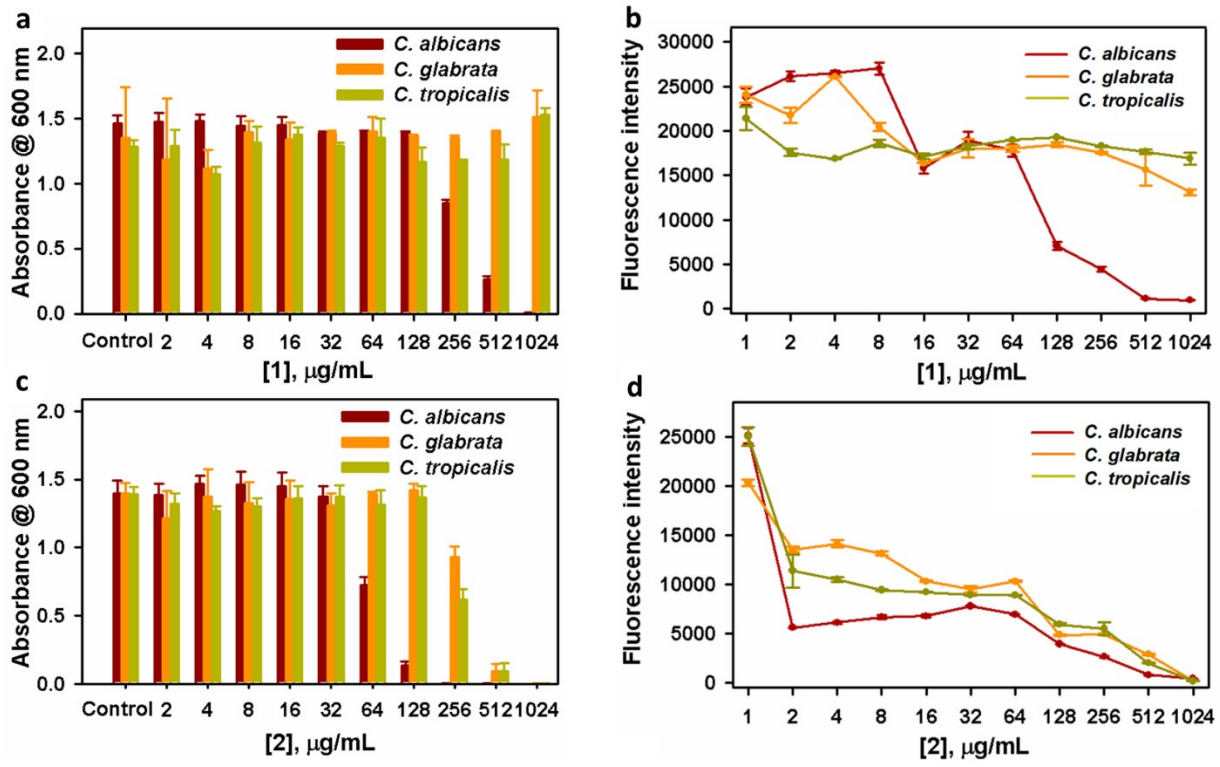

Fig. S13. (a) Anticandidal efficacy of varied concentrations of complex **1** against the growth of fungal strains; **(b)** Metabolic viability of tested fungal strains in treatment with complex **1** as divulged through Alamar blue assay; **(c)** Anticandidal efficacy of varied concentrations of complex **2** against the growth of fungal strains; **(d)** Metabolic viability of tested fungal strains in treatment with complex **2** as divulged through Alamar blue assay.

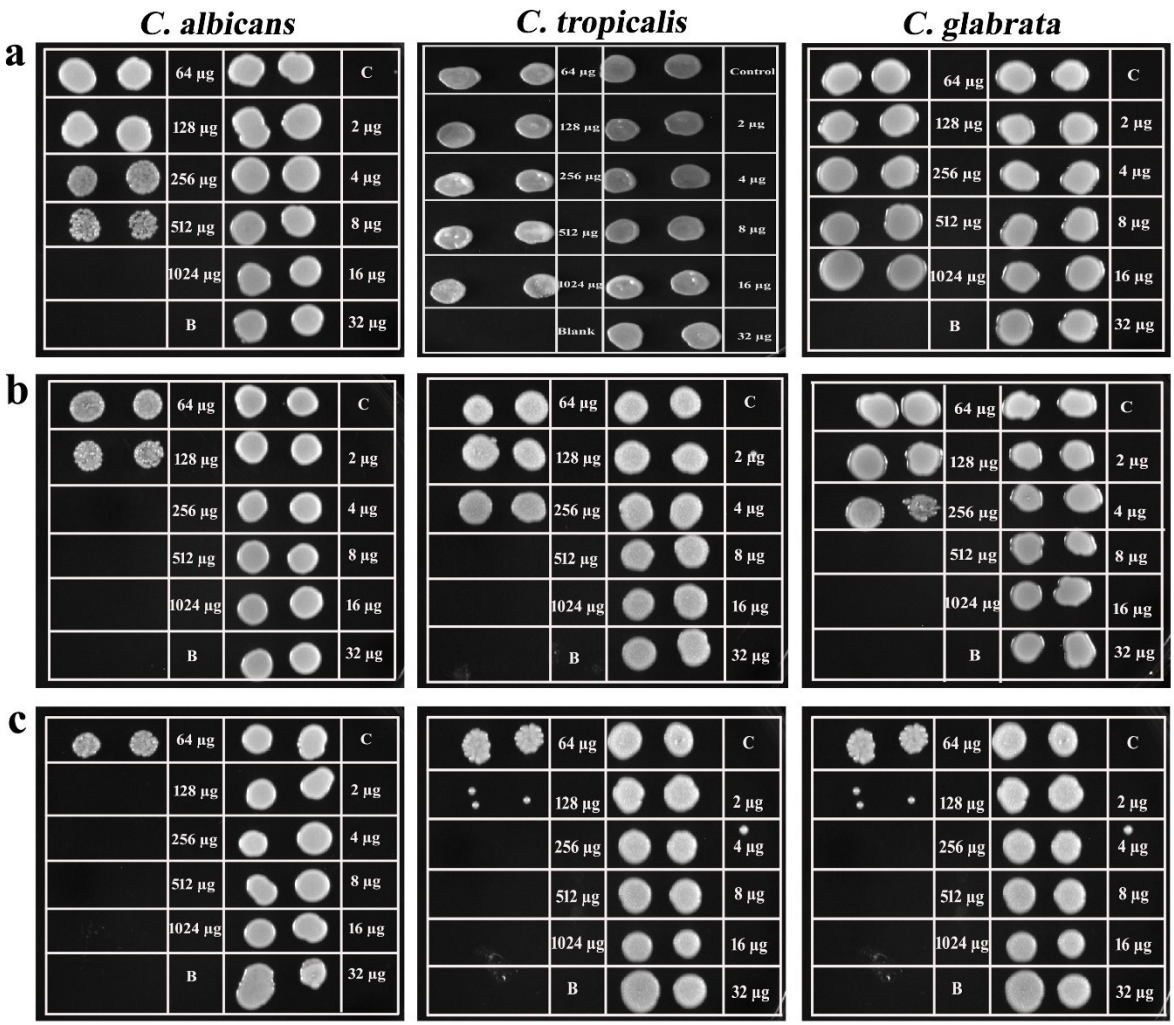

Fig. S14. MFC of complexes **(a) 1**, **(b) 2** and **(c) 3** against three *Candida* species as determined through spot assay.

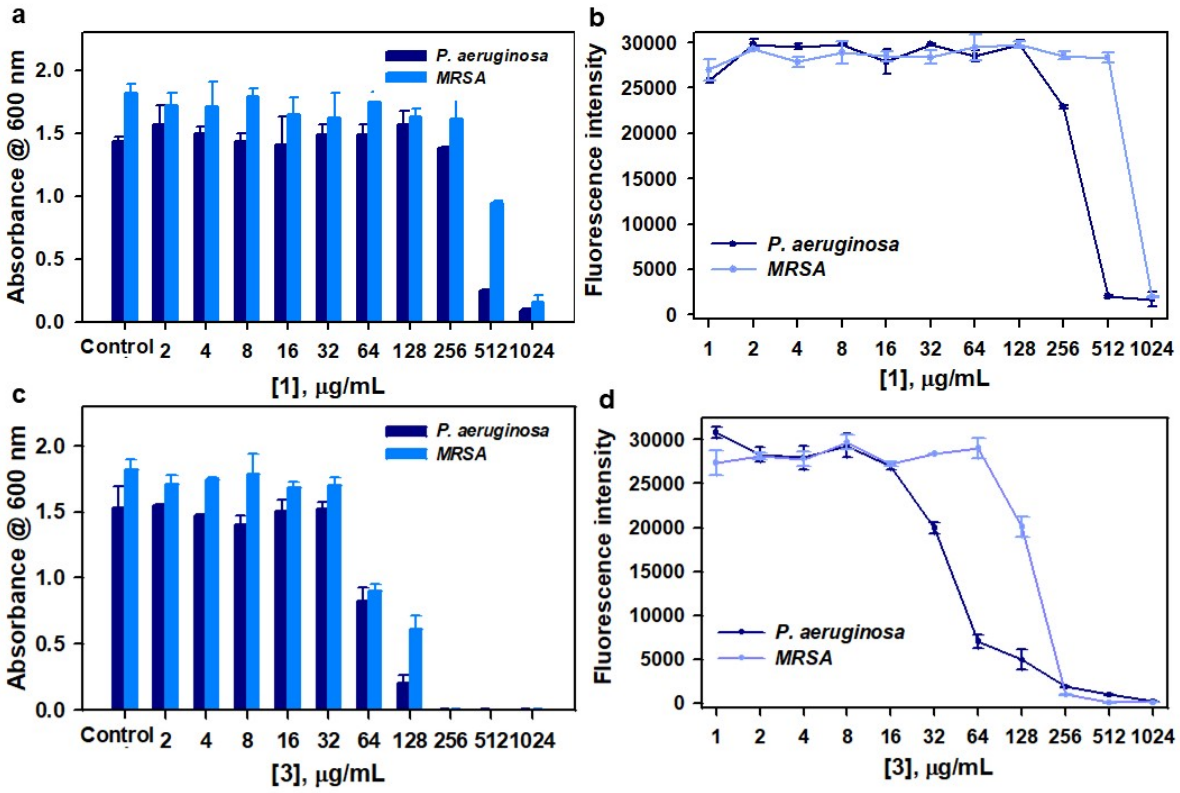

Fig. S15. (a) Antibacterial potency of varied concentrations of complex **1** against planktonic growth of bacterial strains; **(b)** Alamar blue assay demonstrating the actual metabolic state of bacterial strain under treatment with complex **1**; **(c)** Antibacterial potency of varied concentrations of complex **3** against planktonic growth of bacterial strains; **(d)** Alamar blue assay demonstrating the actual metabolic state of bacterial strain under treatment with complex **3**.

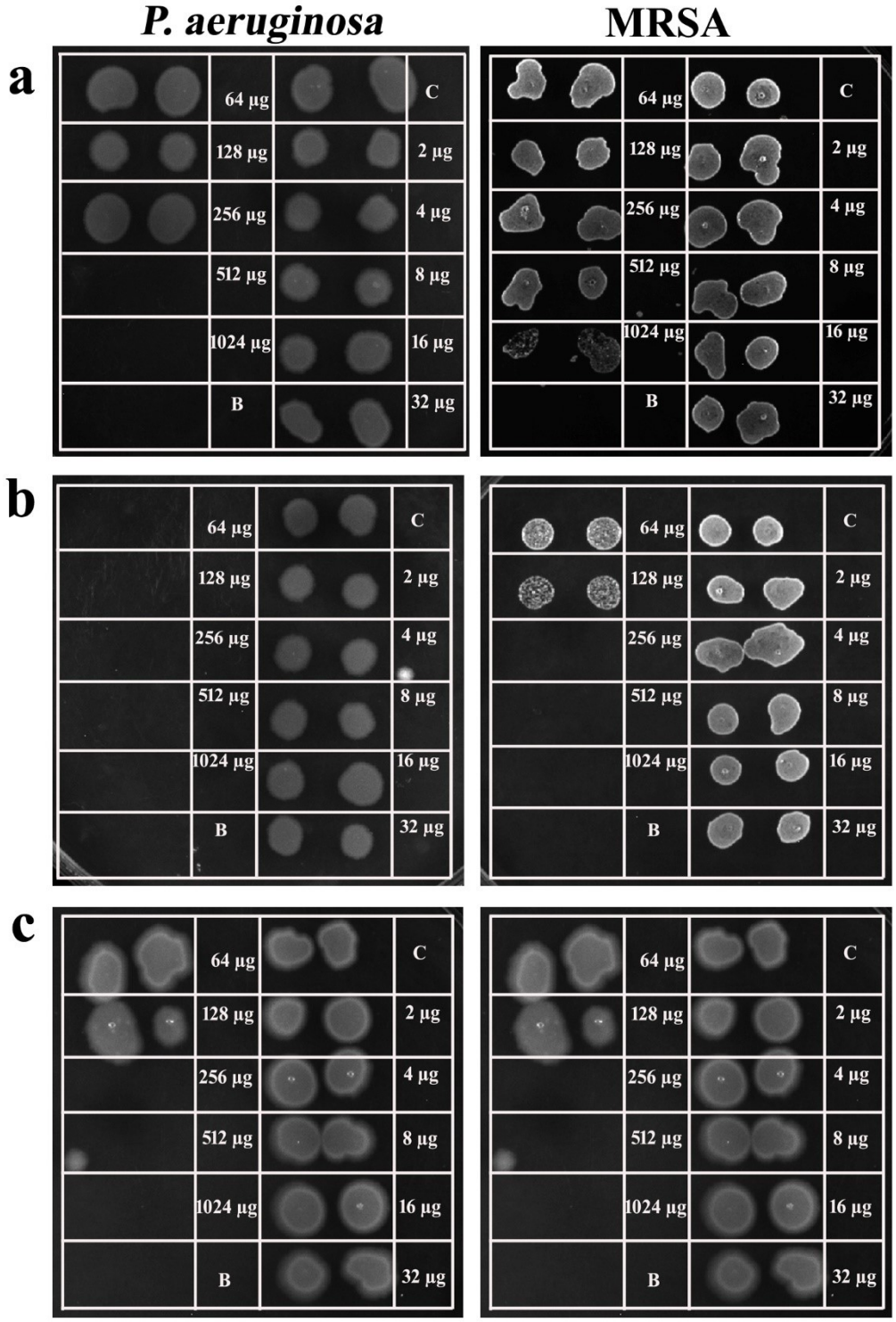

Fig. S16. Spot assay showcased the MBC of complexes **(a) 1**, **(b) 2** and **(c) 3** against two bacterial strains.

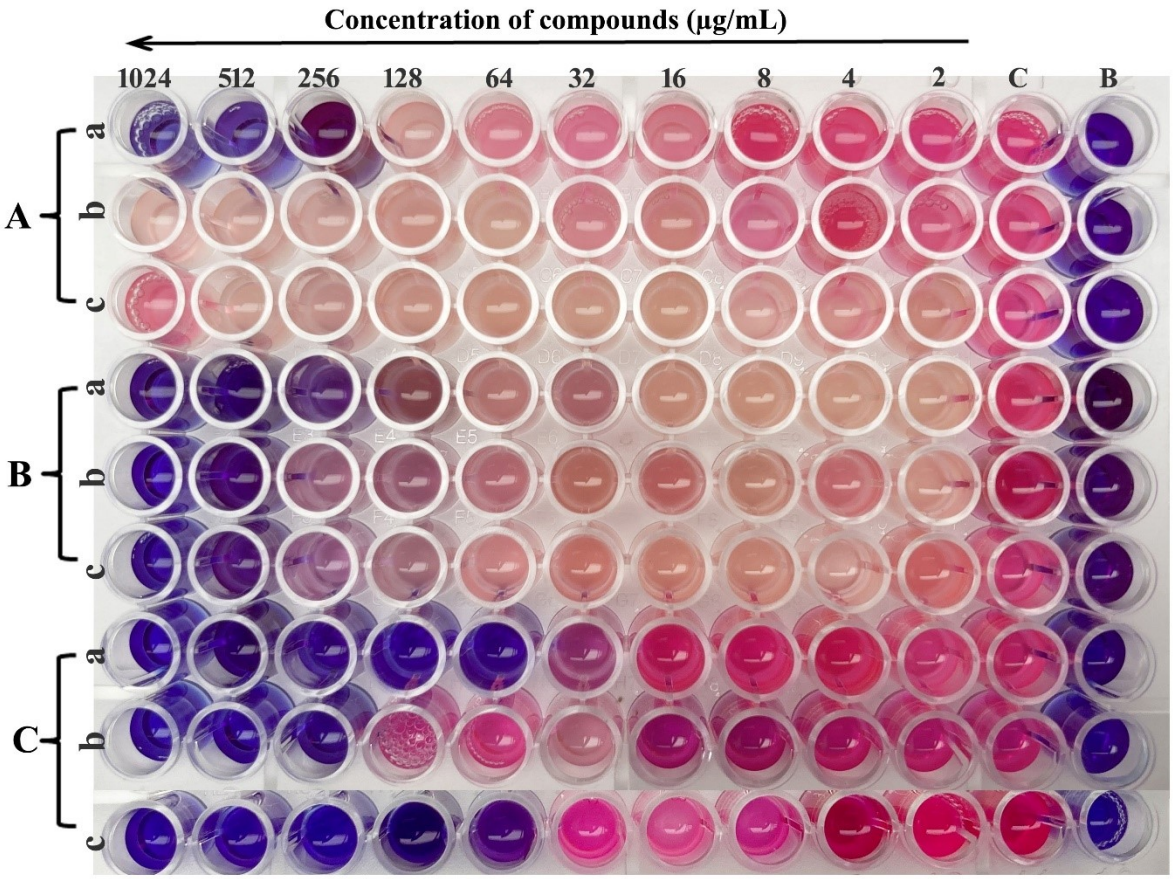

Fig. S17. The representative plate image showcasing the actual metabolic viability of fungal strains under treatment with active complexes. **A**, **B**, and **C** in the graph signify the complexes **1**, **2**, and **3**, respectively. **a**, **b**, and **c** indicate the test organism *C. albicans*, *C. glabrata* and *C. tropicalis*, respectively.

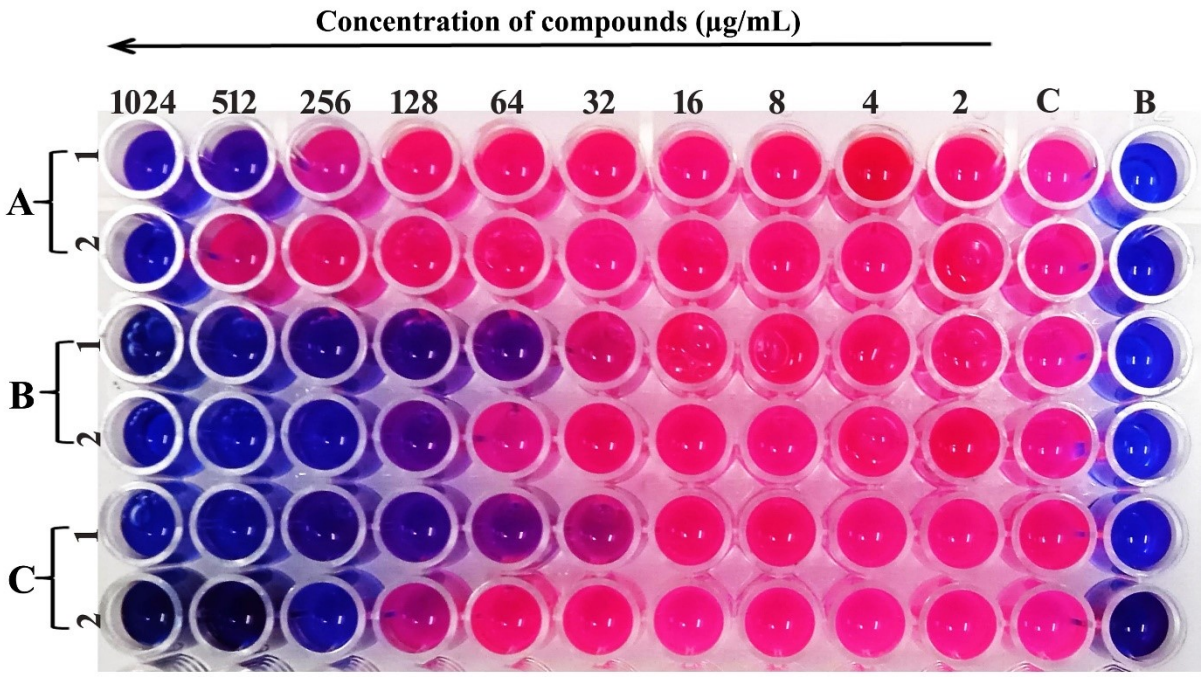

Fig. S18. The representative plate image showcasing the true metabolic viability of bacterial strains under treatment with active compounds. **A**, **B**, and **C** in the graph signify complexes **1**, **2**, and **3**, respectively. The test organisms *P. aeruginosa* and *MRSA* were denoted as **1**, and **2**, respectively.

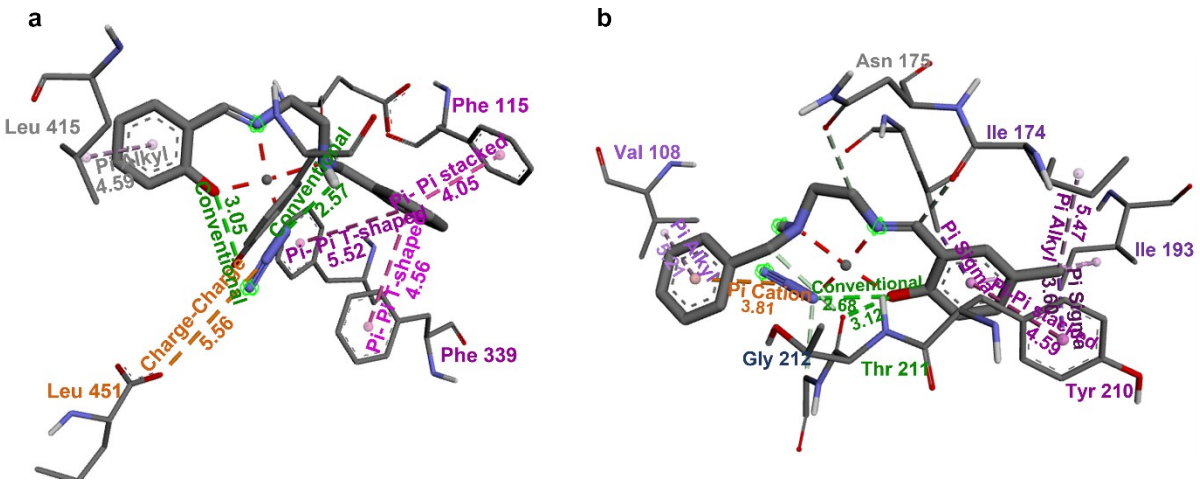

Fig. S19. Two-dimensional view of complexes **(a) 1** and **(b) 2** into the binding cavity of fungal strain *N*-myristoyl transferase (1iyl). The interaction distance is mentioned in Å.

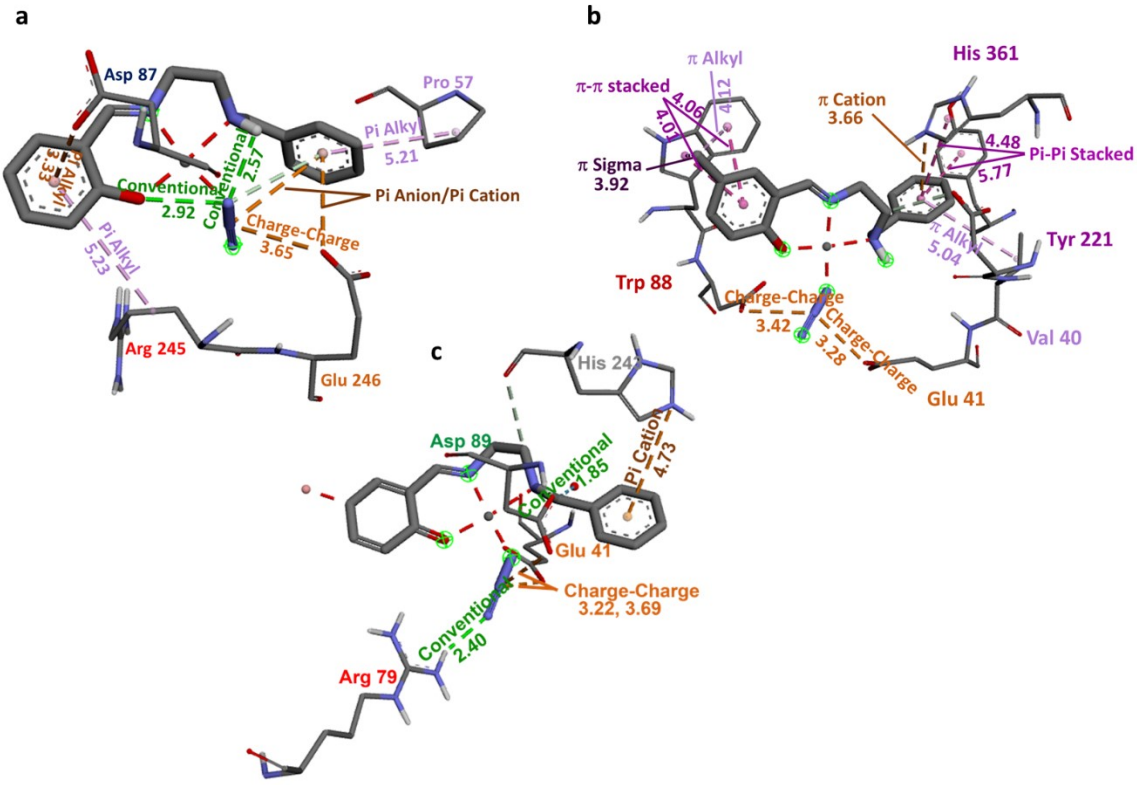

Fig. S20. Two-dimensional view of complexes **(a) 1**, **(b) 2** and **(c) 3** into the binding cavity of bacterial strain aminopeptidase P (5wze). The interaction distance is mentioned in Å.

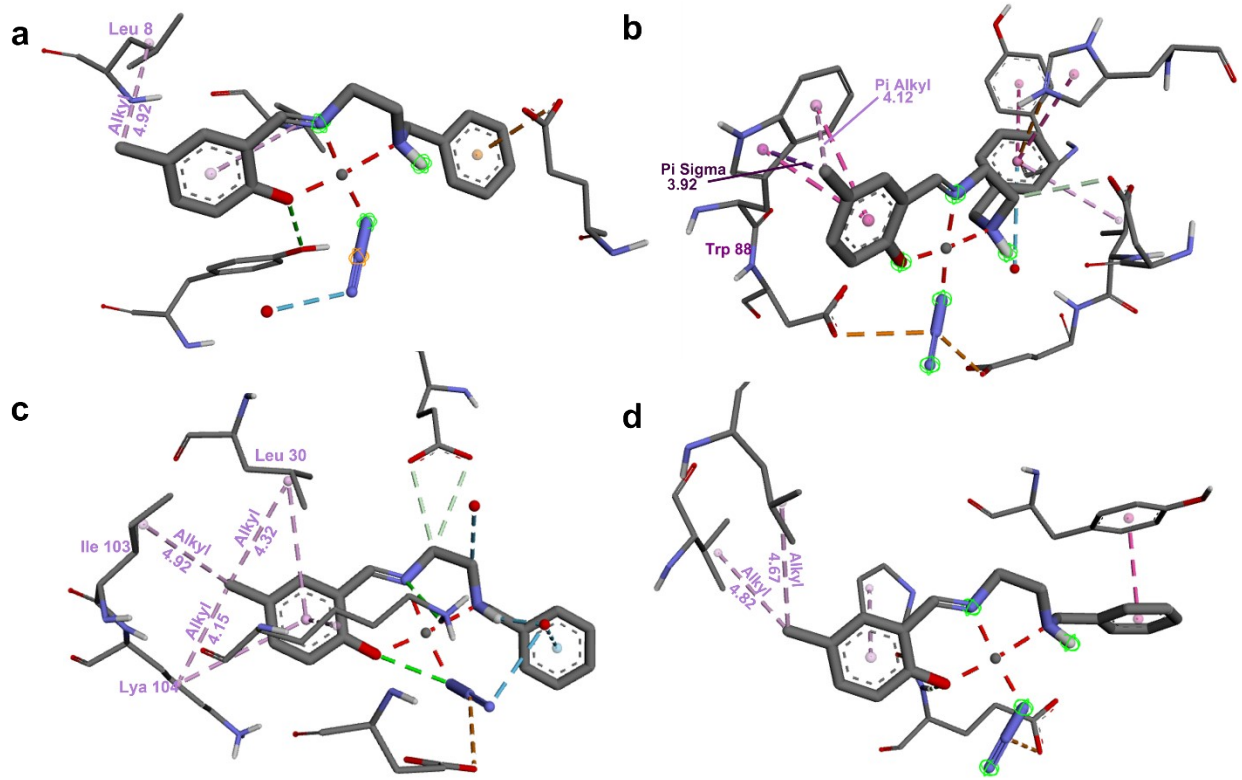

Fig. S21. Two-dimensional view of complex **2** showing non-bonding interactions using methyl moiety into the binding cavity of bacterial strains **(a)** transcriptional activator protein (2uvo) of *P. aeruginosa*; **(b)** aminopeptidase P (5wze) of *P. aeruginosa*; **(c)** protein binding (6p8s) of *P. aeruginosa*; (**d**) transferase (5tze) of *MRSA*. The interaction distance is mentioned in Å.